© 2017. Published by The Company of Biologists Ltd | Development (2017) 144, 837-843 doi:10.1242/dev.141309

RESEARCH REPORT

# Growth control in the *Drosophila* eye disc by the cytokine Unpaired

**Jannik Vollmer[1,2], Patrick Fried[1,2], Daniel Aguilar-Hidalgo[3,*], Máximo Sánchez-Aragón[3], Antonella Iannini[3], Fernando Casares[3,‡] and Dagmar Iber[1,2,‡]**

## ABSTRACT

A fundamental question in developmental biology is how organ size is controlled. We have previously shown that the area growth rate in the *Drosophila* eye primordium declines inversely proportionally to the increase in its area. How the observed reduction in the growth rate is achieved is unknown. Here, we explore the dilution of the cytokine Unpaired (Upd) as a possible candidate mechanism. In the developing eye, *upd* expression is transient, ceasing at the time when the morphogenetic furrow first emerges. We confirm experimentally that the diffusion and stability of the JAK/STAT ligand Upd are sufficient to control eye disc growth via a dilution mechanism. We further show that sequestration of Upd by ectopic expression of an inactive form of the receptor Domeless (Dome) results in a substantially lower growth rate, but the area growth rate still declines inversely proportionally to the area increase. This growth rate-to-area relationship is no longer observed when Upd dilution is prevented by the continuous, ectopic expression of Upd. We conclude that a mechanism based on the dilution of the growth modulator Upd can explain how growth termination is controlled in the eye disc.

**KEY WORDS: Eye disc development, Growth control, Upd, Dilution**

## INTRODUCTION

How organs measure their growth to control their final size is still an open question in biology. The primordia of the adult organs in *Drosophila*, the imaginal discs, present an attractive model system to address this question (Hariharan, 2015; Mirth and Shingleton, 2012). We recently found that the area growth rate of the *Drosophila* eye disc declines inversely proportionally to the increasing eye disc area (Vollmer et al., 2016). An inverse relationship between the growth rate and the total area could arise if a long-lived, diffusible, extracellular growth factor was diluted as the organ grows, because then dilution would reduce the concentration of this factor proportionally to the increase in eye disc area. The expression of such a growth factor would need to cease before the eye disc growth process starts to set an initial concentration. The factor would then need to be sufficiently long-lived to be diluted rather than degraded and the cellular response would need to be linearly related to the concentration. The factor would further need to be extracellular and diffusible because the growth rate declines uniformly, while cell division patterns are non-uniform in the eye disc (Wartlick et al., 2014; Wolff and Ready, 1991). To avoid loss of the extracellular factor from the eye disc over developmental time, it would need to act on the apical side, which faces the closed luminal space of the disc. Finally, dispersal of the growth factor would need to be limited to an area close to the apical cell membrane, so that it would be diluted relative to the area.

Mutations in the JAK/STAT pathway, such as the loss or overexpression of its ligand Unpaired (Upd; Upd1 – FlyBase), are known to alter the size of the eyes without affecting eye disc patterning (Bach et al., 2003; Juni et al., 1996). Intriguingly, most of the above requirements for a factor controlling growth by dilution have already been reported for the cytokine Upd. Thus, Upd is expressed in the posterior margin of the eye disc in late second/early third larval stage, but its expression stops as soon as the differentiation of the posterior cells starts behind the differentiation front, called the morphogenetic furrow (MF) (Bach et al., 2007). In spite of the production stop, Upd as well as its intracellular response factor pSTAT (phosphorylated Stat92E) can still be detected with antibody staining 24-48 h after Upd production has ceased (Zhang et al., 2013). A GFP-tagged Upd has been shown to diffuse extracellularly (Tsai and Sun, 2004), and extracellular Upd and its downstream signalling factor, pSTAT, can indeed be detected uniformly in the entire wild-type eye and antenna discs by antibody staining (Zhang et al., 2013). Moreover, the JAK/STAT pathway responds approximately linearly to the Upd concentration in cell culture assays (Harrison et al., 1998; Wright et al., 2011). Finally, Upd has been found associated to the apical extracellular matrix (ECM), both in cell culture and in the eye disc (Harrison et al., 1998; Hombría et al., 2005; Zhang et al., 2013), and alterations of the ECM affect the Upd concentration in the ECM and its signalling capability (Zhang et al., 2013).

Here, we combine computational modelling, gene expression manipulations and quantitative measurements to test the Upd dilution-based mechanism. We find that the growth kinetics in Upd mutants are quantitatively consistent with the predictions of an area-dependent dilution mechanism, and that the stability of Upd is sufficient for a dilution mechanism. We conclude that a Upd-based dilution mechanism for organ growth control is plausible.

## RESULTS AND DISCUSSION

We combined genetic perturbations and mathematical modelling to test the Upd-dependent dilution mechanism for growth control. To this end, we measured and simulated the effects of either lowering Upd availability or increasing Upd production ectopically and continuously, thereby counteracting dilution (Fig. 1A). As described before (Vollmer et al., 2016), we measured the total area, $T$, as well as the posterior, $P$, and anterior, $A$, areas (Fig. 1B) during eye disc development, using both 2D projections and 3D renderings of the imaged eye discs (Fig. S1; see Materials and

[1]Department of Biosystems, Science and Engineering (D-BSSE), ETH Zurich, Mattenstraße 26, Basel 4058, Switzerland. [2]Swiss Institute of Bioinformatics (SIB), Mattenstraße 26, Basel 4058, Switzerland. [3]Department of Gene Regulation and Morphogenesis, CABD, Universidad Pablo de Olavide, Seville 41013, Spain. *Present address: Department of Biological Physics, Max Planck Institute for the Physics of Complex Systems, Dresden 01187, Germany.

‡Authors for correspondence (fcasfer@upo.es; dagmar.iber@bsse.ethz.ch)

D.I., 0000-0001-8051-1035

**Received 20 June 2016; Accepted 10 January 2017**

Development (2017) 144, 837-843 doi:10.1242/dev.141309

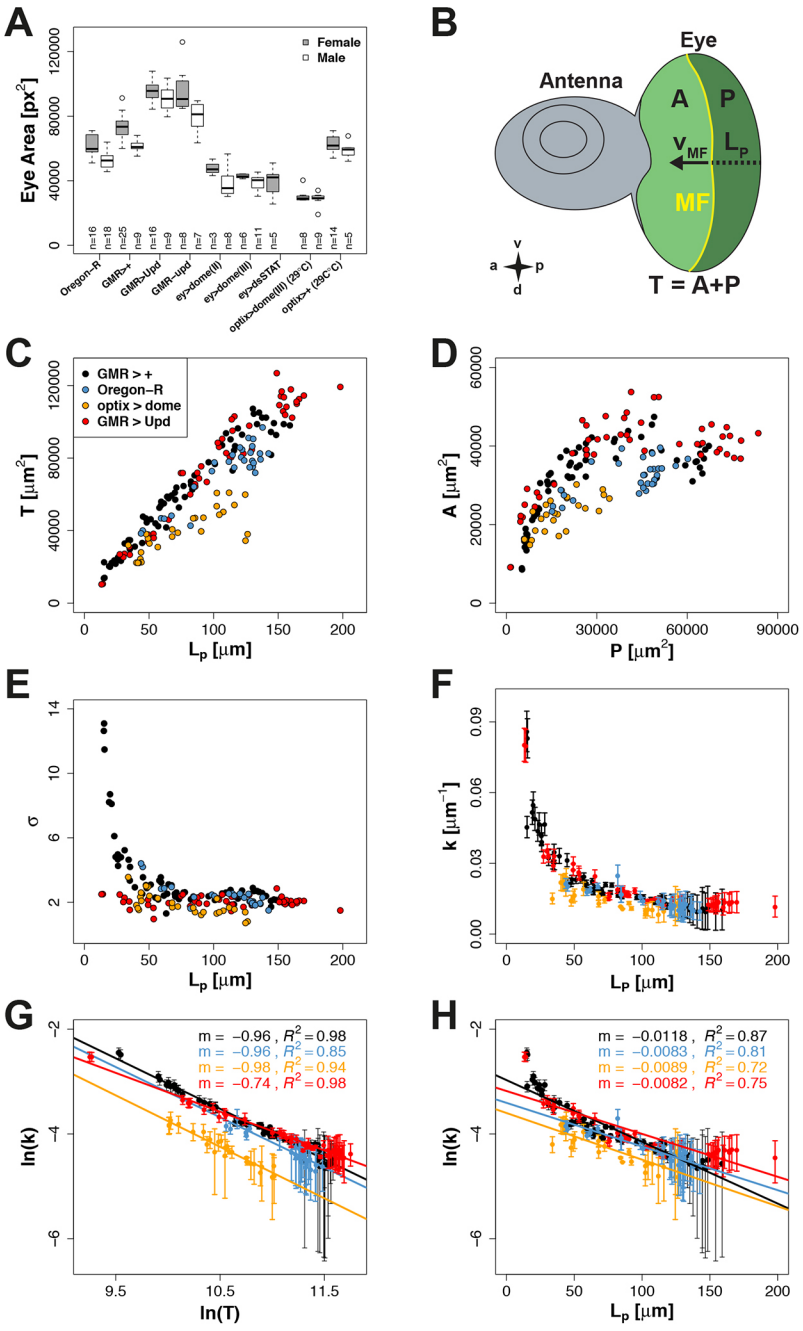


**Fig. 1. Growth kinetics in differently sized *Drosophila* strains.** (A) Boxplots of eye sizes in adult flies. Genotype (wild type or perturbations in the JAK/STAT signalling pathway), sex, and sample sizes are indicated. Full descriptions of genotypes are given in Materials and Methods. (B) Scheme of an eye-antenna imaginal disc with the characteristic measures. P, posterior area (dark green); A, anterior area (light green); T, total area; $L_P$, posterior length; MF, morphogenetic furrow (yellow); $v_{MF}$, speed of the MF. (C,D) Growth kinetics of eye imaginal discs in the different genotypes. (E,F) Axis ratio σ and area growth rate *k* (shown as mean±s.d.; Fig. S3) during eye disc development. (G,H) ln-ln plot of the growth rate *k* versus total area *T*, and ln-linear plot versus posterior length $L_P$ (mean± s.d.). The data for Oregon-R and *GMR-GAL4* (‘*GMR*>+’) were reproduced from Vollmer et al. (2016).

Methods and supplementary Materials and Methods). Here, the posterior length $L_P$ (Fig. 1B, dashed line) can be used as a measure of developmental progress (Vollmer et al., 2016; Wartlick et al., 2014).

### Upd sequestration leads to slower growth, but maintains area dependency of growth rate

First, we reduced the concentration of available Upd in the developing eye by expressing a truncated form of its receptor *dome* (domeΔCYT), which sequesters Upd (Brown et al., 2001), or inhibited signal transduction by expressing a STAT-specific RNAi (see Materials and Methods for details) (Fig. 1A). All genetic combinations tested resulted in smaller adult eyes. As eye reduction was strongest in *optix-GAL4; UAS-domeΔCYT* (‘*optix>dome*’; Fig. 1A), we continued with this genotype. Compared with *GMR>+* and Oregon-R control discs (Vollmer et al., 2016), the total area growth, relative to MF advancement (as measured by $L_P$) is slower in *optix>dome* eye discs (Fig. 1C), and these discs have smaller anterior and posterior areas (Fig. 1D). A difference in the growth rate could, in principle, result from a difference in eye disc shape: for the same initial total area, more elongated eye discs grow to a smaller final size (Fig. S2). However, the *optix>dome* eye discs are, if anything, rounder than the control strains (Fig. 1E; supplementary Materials and Methods). Therefore, a shape difference cannot explain the observed difference in the growth rate.

We next checked whether the area growth rate would still decline inversely proportionally with the (more slowly) increasing eye disc area in the *optix>dome* mutant eye disc. As introduced previously

Development (2017) 144, 837-843 doi:10.1242/dev.141309

(Vollmer et al., 2016), the area growth rate can be determined as

$$k(L_P) = \frac{dT}{dL_P}/A. \quad (1)$$

Here, we assumed that the area growth rate, $k$, is linearly related to the Upd concentration, given the established linear relationship between the Upd concentration and the cellular STAT response (Harrison et al., 1998; Wright et al., 2011). As previously described (Vollmer et al., 2016), the derivative $\frac{dT}{dL_P}$ was determined by fitting the data in Fig. 1C with splines (Fig. S3). We could then use a diagnostic *ln(k)* versus *ln(T)* plot of the data to evaluate the plausibility of area-dependent growth control (P_A), i.e.

$$k(L_P) = k_0 \frac{T(0)}{T(L_P)} \quad (2)$$

for the different genotypes (Fig. 1G). To support an area-dependent growth law, the *ln(k)* versus *ln(T)* plots should be fitted by straight lines of slope minus one. As we showed before, the slope is indeed very close to minus one (−0.96) for the Oregon-R control strain (Vollmer et al., 2016). Intriguingly, the slope is very close to minus one (−0.98) also for the *optix>dome* strain, even though the eye discs of the *optix>dome* strain differ substantially in total size (Fig. 1C) and in the anterior area (Fig. 1D) over developmental time, and there are no correlated changes between $\frac{dT}{dL_P}$ and $A$ (Fig. S4), thus pointing to distinct underlying growth kinetics in the different genotypes.

### Sustained Upd expression leads to a slower decline in the growth rate

We next tested whether the cells in the anterior eye discs remain sensitive to changes in the Upd concentration throughout eye disc

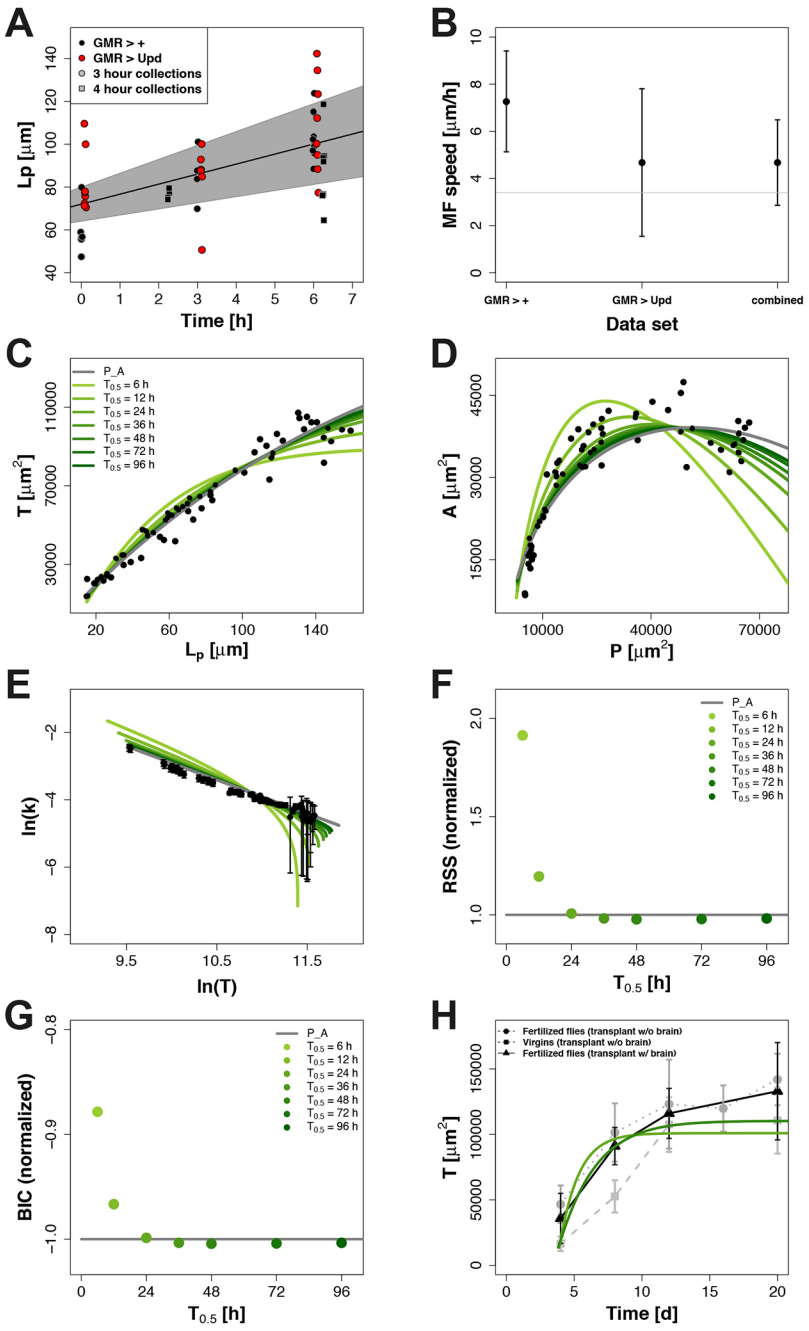


**Fig. 2. Impact of Upd stability.** (A) The position of the MF, i.e. the posterior length (*Lp*), at the indicated time intervals in GMR>+ (black) and GMR>Upd (red) eye discs. Egg collection intervals were 3 h (circles) or 4 h (squares). The black line shows the linear fit of the combined data sets. The grey area indicates the 95% confidence interval. Egg collection and larval rearing was at 25°C; the last time point corresponds to the time of pupariation initiation (120 h after egg laying at 25°C). (B) Inferred MF speed in the GMR>+, the GMR>Upd, and the combined data set. Error bars indicate 95% confidence intervals. The grey line marks the previously inferred MF speed of 3.4 µm/h (Vollmer et al., 2016; Wartlick et al., 2014). (C,D) Best fits of the model (Eqn. 4; supplementary Materials and Methods) with different half-lives to the measured total and anterior-posterior areas in *GMR>+*. P_A, area-dependent model (Eqn. 2). Parameter values are given in Table S1. (E) Comparison of the growth rates predicted by the model for the different half-lives (lines) to the data-inferred growth rate (dots, mean±s.d.) in *GMR>+*. (F) Deviation of the model from the datasets as measured by the residual sum of squares (RSS) versus the half-life used in the model. The values were normalized to the RSS obtained from fitting the pure dilution model (P_A; Eqn. 2). Parameters for the different models are given in Table S1. Grey line, RSS for a pure dilution model (P_A; Eqn. 2). (G) Bayesian information criterion (BIC) versus the half-life. Values were normalized to the BIC obtained for a pure dilution model (P_A; Eqn. 2). BIC was calculated as $BIC = n \cdot \ln\left(\frac{RSS}{n}\right) + k \cdot \ln(n)$, where RSS is the residual sum of squares, $n$ is the number of data points and $k$ the number of parameters being estimated. Grey line, BIC for a pure dilution model (P_A; Eqn. 2). (H) The substantially slower growth kinetics of transplanted imaginal discs (supplementary Materials and Methods) (Garcia-Bellido, 1965) can be matched by the area-dependent growth model (Eqn. 4) with an Upd half-life of 24 h, and slightly better with 48 h. To reproduce the slow eye disc development, the MF speed $v_{MF}$ had to be lowered to 5% of the value used for *GMR>+*. The initial growth rate, $k_0$, had to be lowered to 28% or 18% for a half-life of 24 h or 48 h, respectively. Relative values are given with respect to Table S1. Here, we note that the reported measurements are based on 2D measurements and include the entire eye-antennal disc (Garcia-Bellido, 1965). In our control strains, 2D and 3D measurements are very well correlated with $T_{3D}$=1.6×$T_{2D}$ (Fig. S1) (Vollmer et al., 2016) and the eye disc covers 60% of the entire eye-antennal disc such that the two effects cancel each other out.

Development (2017) 144, 837-843 doi:10.1242/dev.141309

development. To this end, we determined the area growth rate, $k$, in eye discs in which Upd was expressed ectopically in differentiating cells posterior to the MF (*GMR>Upd*; Fig. S3). Such overexpression has been shown before to result in large eyes (about 1.3-fold larger than control eyes, Fig. 1A) (Bach et al., 2003; Tsai and Sun, 2004). We find that the *GMR>Upd* eye discs grow very similarly to *GMR>+* control discs (Fig. 1C,D), except that the eye discs of *GMR>Upd* larvae are rounder initially (Fig. 1E) and their area becomes larger eventually (Fig. 1C), demonstrating that the eye discs remain sensitive to the Upd concentration also at later stages.

The very good fit of a straight line with slope minus one to the control and *optix>dome* data in the *ln(k)* versus *ln(T)* plot (Fig. 1G) strongly supported an area-dependent growth rate. Intriguingly, in case of the *GMR>Upd* strain, the slope is −0.74, i.e. $k(L_P) = k_0\left(\frac{T(0)}{T(L_P)}\right)^{0.74}$ (Fig. 1G, red), which indicates a delayed reduction in the growth rate as *GMR>Upd* eye discs grow. Importantly, consistent with model predictions, the initial decline in the growth rate is very similar in *GMR>+* and *GMR>Upd* eye discs. Thus, when we add Upd to a recently published model of eye disc development (Fried et al., 2016), the model predicts a similar initial decline in the Upd concentration in both control and *GMR>Upd* eye discs (Fig. S5). This is so because in *GMR>Upd* discs Upd production behind the MF is very low in early stages (when the number of GMR-expressing cells is still small), but the effect of dilution is strongest at early stages because the area fold-increase is fastest initially. We conclude that the growth rates that are obtained with a continued ectopic expression of Upd behind the MF are consistent with growth control by dilution.

Finally, we note that the data in a *ln(k)* versus $L_p$ plot are also fitted reasonably well by straight lines, which would correspond to an exponential decline in the growth rate

$$k(L_P) = e^{-\delta(L_P - L_P(0))}, \quad (3)$$

as could result from the linear decay of a growth factor (Fig. 1H) (Vollmer et al., 2016). However, the fit is consistently worse, particularly for early and late data points (Fig. 1H; Fig. S6). In conclusion, an area-dependent decline fits the data slightly better than an exponential decline.

### A quantitative analysis of the required Upd stability and spreading

Independently of dilution, all proteins decay over time. As a result of Upd degradation and dilution, we then have for the area growth rate

$$k(L_P) = k_0 \frac{T(0)}{T(L_P)} e^{-\delta(L_P - L_P(0))}, \quad (4)$$

where $\frac{T(0)}{T(L_P)}$ represents the dilution effect, and $e^{-\delta(L_p - L_p(0))}$ incorporates turnover of Upd at rate $\delta$. We can use the constant speed of the MF (Wartlick et al., 2014) to convert the degradation rate to time (Vollmer et al., 2016). We measured the speed of the MF in GMR>+ eye discs as 7.3±2.1 µm/h (mean±s.d.) and in GMR>Upd discs as 4.7±3.1 µm/h (Fig. 2A,B), which is similar to

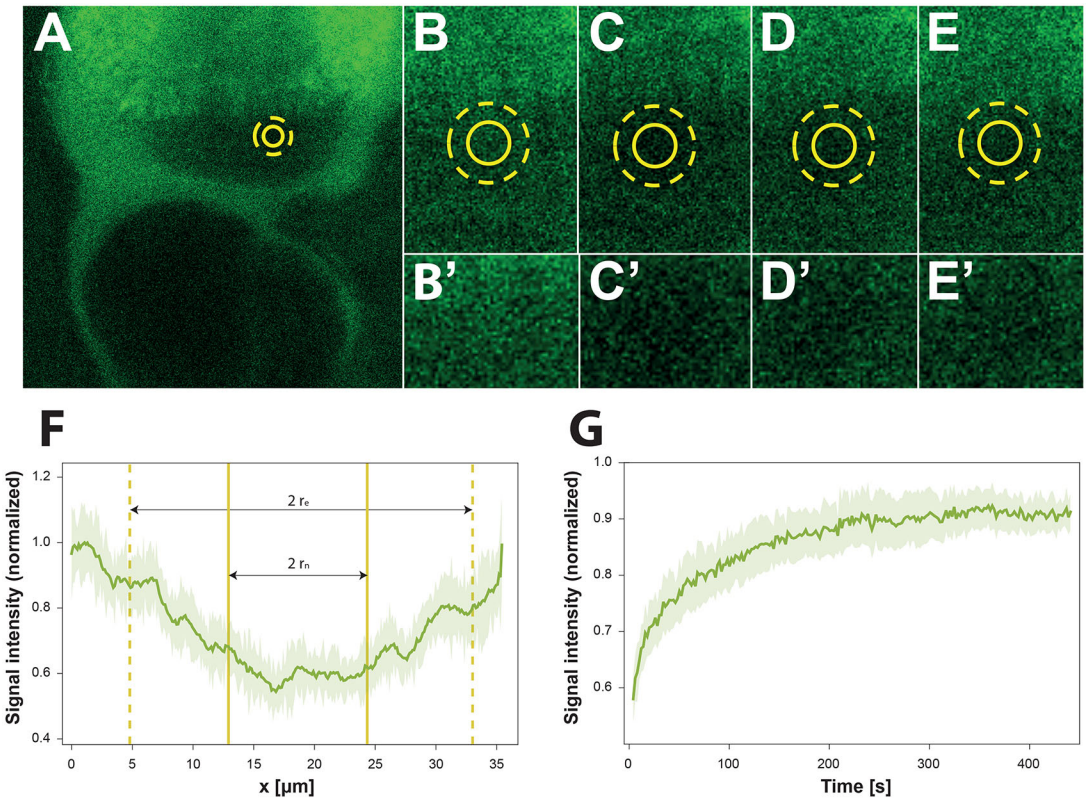


**Fig. 3. The diffusion coefficient of Upd.** (A) Eye imaginal disc from GMR-GAL4; UAS-GFP:Upd. The ROI selected for photobleaching is marked (yellow circle). (B-E′) Magnification of ROI (photobleached area, solid circle in A) and the surrounding tissue (B-E) before photobleaching (B), directly after photobleaching (C), and at *t*=100 s (D) and *t*=250 s (E). Panels B′-E′ show a magnification of the photobleached area (solid circles in panels B-E) at the same time points. (F) Normalized mean intensity of the bleached profile. $2r_n$, nominal diameter (ROI); $2r_e$, effective diameter. (G) Recovery dynamics of the mean GFP signal normalized to pre-bleached intensity. In F,G, shaded area shows s.e.m.

Development (2017) 144, 837-843 doi:10.1242/dev.141309

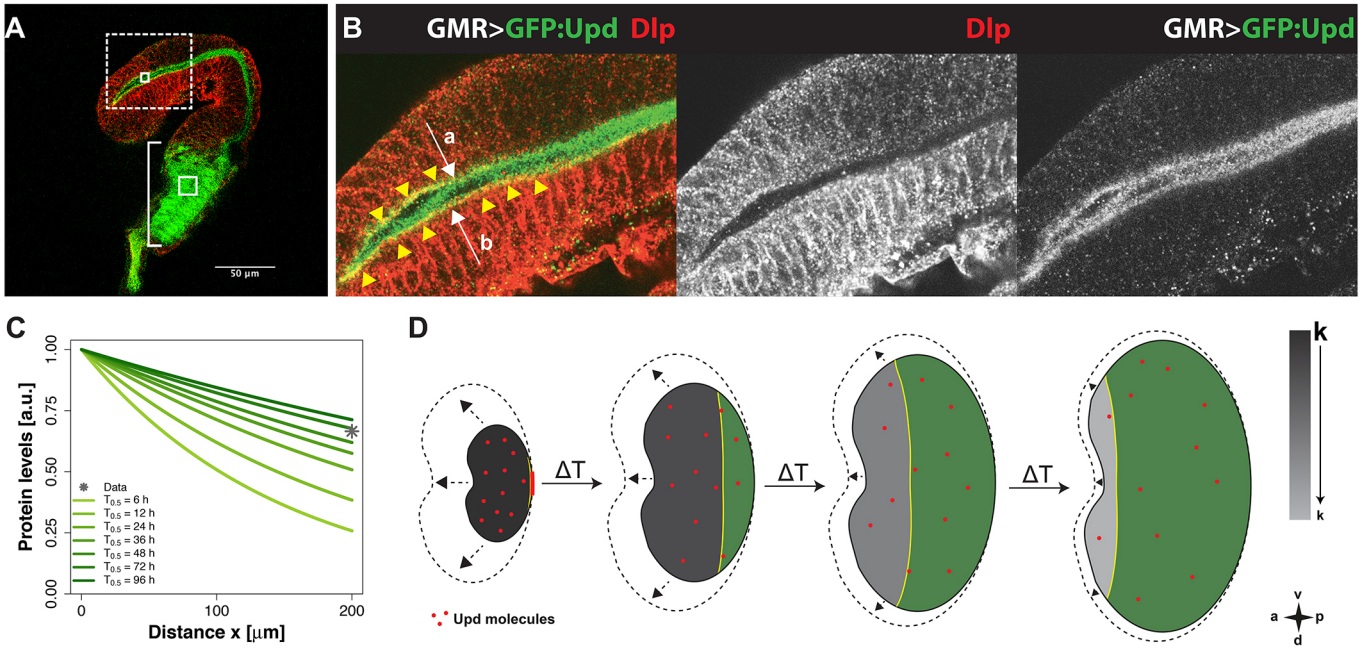


**Fig. 4. Dispersal of Upd.** (A) Confocal optical section of a *GMR>GFP:Upd* disc (GFP signal shown in green), additionally stained for the proteoglycan Dally-like protein (Dlp; red). The GFP:Upd-producing domain is indicated by the vertical bracket. The region marked by the dashed box is magnified in B. (B) Magnification of the disc shown in A. Arrows point from the basal (b) to the apical (a) sides of the epithelium. GFP:Upd is detected on the apical cell surface, colocalizing with Dlp (visualized as yellow signal; marked by yellow arrowheads), as well as in the apical luminal space. (C) Predicted steady-state gradients ($\frac{c}{c_0} = e^{-x/\lambda}, = \sqrt{D/\delta}$) with the measured Upd diffusion coefficient, $D$=0.7 µm$^2$/s, for different Upd half-lives, $T_{0.5}$ [$\delta = ln(2)/T_{0.5}$] (green lines). (D) Graphical summary of the dilution-based growth control mechanism. In the early stages of eye disc development, Upd molecules (red points) are produced at the posterior margin (red line) and spread over the small eye disc domain by diffusion. Upd production ceases at the onset of MF movement. As a result of the increase in the total eye disc area over time, the Upd concentration decreases by dilution. The growth rate, $k$, in the part anterior to the MF is directly proportional to the concentration of Upd (visualized from dark to light grey) and therefore declines inversely proportionally to the change in the total eye disc area. Thus, in the same time span, ΔT, the area increase is less, allowing the MF to catch up and terminate growth. Anterior is to the left, and posterior to the right. Green, posterior area; yellow, MF; dashed lines, growth within the next time step.

but slightly faster than previous reports (Wartlick et al., 2014). Because the linear movement of the MF can be explained with the dynamics of the Hedgehog (Hh)-Decapentaplegic (Dpp) patterning network (Fried et al., 2016), and *upd* mutants do not show patterning defects (Bach et al., 2003), MF movement was not expected to be strongly affected in *upd* mutants. With this MF speed, we require a Upd half-life, $T_{0.5} = \frac{\ln(2)}{\delta}$, of at least 24 h to obtain a good fit between measured and simulated eye disc growth (Fig. 2C-G). Growth was simulated using $\frac{dT}{dL_P} = k(L_P) \cdot A$ and the growth rate in Eqn. 4 (supplementary Materials and Methods) (Vollmer et al., 2016). For slower eye disc development, the required Upd half-life would be longer, and the minimal required Upd stability is therefore dictated by the slowest observed developmental progress. *Drosophila* eye disc development is substantially slowed down in eye discs that are grafted to adult female hosts, where they take almost 2 weeks to achieve their final size (Garcia-Bellido, 1965) (Fig. 2H). The dilution-based growth mechanism recapitulates the observed growth kinetics with an Upd half-life of 24 h reasonably well, but a better fit is obtained with a half-life of 48 h (Fig. 2H; supplementary Materials and Methods).

To establish the effective Upd turnover rate, $\delta$, we measured the dispersion of GFP-tagged Upd (Tsai and Sun, 2004) and its effective diffusion coefficient, $D$, using fluorescence recovery after photobleaching (FRAP) in eye discs of *GMR>Upd-GFP* larvae. The FRAP-measured Upd diffusion coefficient, $D$=0.7 µm$^2$/s (Fig. 3; see Materials and Methods and supplementary Materials and Methods for details), is higher than previously published FRAP-measured diffusion coefficients for other diffusible molecules in the ECM of *Drosophila* imaginal discs (0.04-0.1 µm$^2$/s) (Kicheva et al., 2007). To determine a lower boundary on the Upd half-life, we compared the experimentally observed spreading when GFP:Upd is ectopically expressed in different parts of the eye disc (Fig. 4A,B; Fig. S7) with the expected steady state Upd concentration profiles for an effective diffusion coefficient of 0.7 µm$^2$/s and different half-lives (Fig. 4C). In agreement with previous reports (Zhang et al., 2013), we observe Upd-GFP to be essentially uniformly dispersed over a distance of about 100 µm from its expression domain and to decline to about two-thirds of its value in the source within 200 µm from its expression domain (Fig. 4A,C; Fig. S7). The observed shallow gradients all lie above the Upd gradient that would be expected with a half-life of 24 h, and the high Upd concentration at a long distance from the source is best approximated with a half-life of >60 h (Fig. 4C, star). Such an Upd half-life is sufficient to reproduce all measured growth data, including that obtained in *Drosophila* larvae (Fig. 2C-G), and for grafted eye discs (Garcia-Bellido, 1965) (Fig. 2H; supplementary Materials and Methods). It is also consistent with previous reports in which Upd was detected more than 24 h after its production had ceased (Zhang et al., 2013). We note that given the long half-life of the Upd protein, FRAP-based protein stability measurements must be expected to provide underestimates because of bleaching.

Development (2017) 144, 837-843 doi:10.1242/dev.141309

Finally, we note that the localization of Upd mainly in the apical ECM (Fig. 4B) (Harrison et al., 1998; Hombría et al., 2005; Zhang et al., 2013) also means that Upd will not be lost by diffusion out of the eye disc over time, as the apical cell side faces a closed luminal space. This would not be the case if Upd was secreted to the basal ECM.

## Conclusion

We provide evidence that the cytokine Upd fulfils not only qualitatively, but also quantitatively, all requirements for area-dependent growth control of the eye disc based on its rate of dilution. Temporal and spatial changes in the expression of a Upd gene can modulate wing size in wasps (Loehlin and Werren, 2012), suggesting that Upd's role in controlling final organ size might be conserved beyond fruit flies. Variations in the initial amount of Upd could then explain the natural variation in eye size in different dipteran species. Open questions still remain. In particular, although declining growth rates are found throughout developing systems (Grunert et al., 2015; Ricklefs, 2010), the area-dependent growth law that explains the growth kinetics of the *Drosophila* eye discs does not fit the growth data available for the wing disc (Vollmer and Iber, 2016). Therefore, alternative growth control mechanisms need to have evolved as well.

## MATERIALS AND METHODS

### *Drosophila* strains

Oregon-R (Or-R) is a wild-type strain (FlyBase: http://flybase.org). GMR-Upd is a transgenic line in which the GMR-enhancer is linked directly to the *upd* cDNA (Bach et al., 2003). Gene expression manipulation was carried out using the GAL4/UAS system (Brand and Perrimon, 1993). The GAL4 strains used were: *GMR-GAL4* ('*GMR>*'; FlyBase identifier: FBgn0020433), *ey-GAL4* ('*ey>*'; FlyBase identifier: FBtp0012213), *optix2/3-GAL4* ('*optix>*'; Ostrin et al., 2006) and *dpp*-GAL4 (FlyBase identifier: FBti0002123). UAS-strains used were; *UAS-Upd* ('*>Upd*'; Harrison et al., 1998), *UAS-GFP:Upd* ('*>GFP:Upd*'; Tsai and Sun, 2004), *UAS-domeΔCYT*, on either chromosome II or III ['*>dome(II)*' and '*>dome(III)*', respectively; Brown et al., 2001] and *UAS-dsSTAT92E* ('>dsSTAT'; VDRC stock: 43867). All flies were raised on standard media at 25°C unless stated otherwise. All data presented are from female flies/larvae if not stated otherwise.

### Antibody staining, fixation and imaging

Eye imaginal discs were dissected and fixed according to standard protocols (Casares and Mann, 2000). Rabbit anti-aPKC (Abcam AB5813, 1:500), rabbit anti-GFP (Molecular Probes, A11122, 1:1000) and mouse anti-Dlp (13G8; Developmental Studies Hybridoma Bank, 1:5) were used as primary antibodies. Secondary antibodies used were Alexa Fluor 555-conjugated goat anti-rabbit, Alexa Fluor 488-conjugated goat anti-rabbit and Alexa Fluor 568-conjugated goat anti-mouse (Molecular Probes, A21428, A11034 and A11031, respectively; all 1:400). Stained discs were mounted with spacers to prevent flattening and were imaged using a Leica TCS SPE microscope.

### Image analysis

Image analysis was performed as described by Vollmer et al. (2016). See supplementary Materials and Methods for details.

### Computational analysis

Models were simulated and optimized in Matlab R2016a using a forward Euler scheme as described by Vollmer et al. (2016). See supplementary Materials and Methods for details.

### Fluorescence recovery after photobleaching (FRAP)

We followed the same approach as Fried et al. (2016) and we provide a copy of the description in supplementary Materials and Methods. In short, the region of interest (ROI; Fig. 3A) was photobleached using a 488 nm argon laser and recovery was recorded. Following Kang et al. (2012), the diffusion coefficient was calculated as $D_{Upd}$ =0.67±0.19 µm$^2$ s$^{-1}$.

#### Acknowledgements

We thank H. Sun (Academia Sinica, Taipei), E. Bach (Department of Biochemistry and Molecular Pharmacology, NYU, New York) and J.C.-G. Hombría (CABD, Seville) for *Drosophila* stocks and the CABD Advanced Light Microscopy Facility; and C.S. Lopes for participating in initial phases of this work. We thank our colleagues for discussions.

#### Competing interests

The authors declare no competing or financial interests.

#### Author contributions

D.I. and F.C. conceived the study. All authors designed the experiments. F.C., J.V., D.A.-H., M.S.-A. and A.I. acquired experimental data. J.V., F.C., P.F., D.A.-H. and M.S.-A. analysed data. J.V., P.F. and D.I. developed and analysed the model. D.I., F.C. and J.V. wrote the manuscript.

#### Funding

This work was supported by grants from the Ministerio de Economía y Competitividad (Spain) (BFU2012-34324 and BFU2015-66040 to F.C.) and by a Swiss Institute of Bioinformatics Fellowship (to J.V.).

#### Supplementary information

Supplementary information available online at
http://dev.biologists.org/lookup/doi/10.1242/dev.141309.supplemental

#### References

**Abràmoff, M. D., Magalhães, P. J. and Ram, S. J.** (2004). Image processing with ImageJ. *Biophotonics Int.* **11**, 36-42.

**Bach, E. A., Vincent, S., Zeidler, M. P. and Perrimon, N.** (2003). A sensitized genetic screen to identify novel regulators and components of the Drosophila janus kinase/signal transducer and activator of transcription pathway. *Genetics* **165**, 1149-1166.

**Bach, E. A., Ekas, L. A., Ayala-Camargo, A., Flaherty, M. S., Lee, H., Perrimon, N. and Baeg, G.-H.** (2007). GFP reporters detect the activation of the Drosophila JAK/STAT pathway in vivo. *Gene Expr. Patterns* **7**, 323-331.

**Brand, A. H. and Perrimon, N.** (1993). Targeted gene expression as a means of altering cell fates and generating dominant phenotypes. *Development* **118**, 401-415.

**Brown, S., Hu, N. and Hombría, J. C.-G.** (2001). Identification of the first invertebrate interleukin JAK/STAT receptor, the Drosophila gene domeless. *Curr. Biol.* **11**, 1700-1705.

**Casares, F. and Mann, R. S.** (2000). A dual role for homothorax in inhibiting wing blade development and specifying proximal wing identities in Drosophila. *Development* **127**, 1499-1508.

**Coleman, T. F. and Li, Y.** (1996). An interior trust region approach for nonlinear minimization subject to bounds. *SIAM J. Optim.* **6**, 418-445.

**Fried, P., Sánchez-Aragón, M., Aguilar-Hidalgo, D., Lehtinen, B., Casares, F. and Iber, D.** (2016). A model of the spatio-temporal dynamics of Drosophila eye disc development. *PLoS Comput. Biol.* **12**, e1005052.

**Garcia-Bellido, A.** (1965). Larvalentwicklung transplantierter Organe von Drosophila melanogaster im Adultmilieu. *J. Insect Physiol.* **11**, 1071-1078.

**Grunert, L. W., Clarke, J. W., Ahuja, C., Eswaran, H. and Nijhout, H. F.** (2015). A quantitative analysis of growth and size regulation in manduca sexta: the physiological basis of variation in size and age at metamorphosis. *PLoS One* **10**, e0127988.

**Hariharan, I. K.** (2015). Organ size control: lessons from Drosophila. *Dev. Cell* **34**, 255-265.

**Harrison, D. A., McCoon, P. E., Binari, R., Gilman, M. and Perrimon, N.** (1998). Drosophila unpaired encodes a secreted protein that activates the JAK signaling pathway. *Genes Dev.* **12**, 3252-3263.

**Hombría, J. C.-G., Brown, S., Häder, S. and Zeidler, M. P.** (2005). Characterisation of Upd2, a Drosophila JAK/STAT pathway ligand. *Dev. Biol.* **288**, 420-433.

**Juni, N., Awasaki, T., Yoshida, K. and Hori, S. H.** (1996). The Om (1E) mutation in Drosophila ananassae causes compound eye overgrowth due to tom retrotransposon-driven overexpression of a novel gene. *Genetics* **143**, 1257-1270.

**Kang, M., Day, C. A., Kenworthy, A. K. and DiBenedetto, E.** (2012). Simplified equation to extract diffusion coefficients from confocal FRAP data. *Traffic* **13**, 1589-1600.

**Kicheva, A., Pantazis, P., Bollenbach, T., Kalaidzidis, Y., Bittig, T., Jülicher, F. and González-Gaitán, M.** (2007). Kinetics of morphogen gradient formation. *Science* **315**, 521-525.

Development (2017) 144, 837-843 doi:10.1242/dev.141309

**Loehlin, D. W. and Werren, J. H.** (2012). Evolution of shape by multiple regulatory changes to a growth gene. *Science* **335**, 943-947.

**Mirth, C. K. and Shingleton, A. W.** (2012). Integrating body and organ size in Drosophila: recent advances and outstanding problems. *Front. Endocrinol.* **3**, 49.

**Neto, M., Aguilar-Hidalgo, D. and Casares, F.** (2016). Increased avidity for Dpp/BMP2 maintains the proliferation of progenitors-like cells in the Drosophila eye. *Dev. Biol.* **418**, 98-107.

**Ostrin, E. J., Li, Y., Hoffman, K., Liu, J., Wang, K., Zhang, L., Mardon, G. and Chen, R.** (2006). Genome-wide identification of direct targets of the Drosophila retinal determination protein Eyeless. *Genome Res.* **16**, 466-476.

**Ricklefs, R. E.** (2010). Embryo growth rates in birds and mammals. *Funct. Ecol.* **24**, 588-596.

**Staehling-Hampton, K., Jackson, P. D., Clark, M. J., Brand, A. H. and Hoffmann, F. M.** (1994). Specificity of bone morphogenetic protein-related factors: cell fate and gene expression changes in Drosophila embryos induced by decapentaplegic but not 60A. *Cell Growth Differ.* **5**, 585-593.

**Tsai, Y.-C. and Sun, Y. H.** (2004). Long-range effect of upd, a ligand for Jak/STAT pathway, on cell cycle in Drosophila eye development. *Genesis* **39**, 141-153.

**Vollmer, J. and Iber, D.** (2016). An unbiased analysis of candidate mechanisms for the regulation of Drosophila wing disc growth. *Sci. Rep.* **6**, 39228.

**Vollmer, J., Fried, P., Sánchez-Aragón, M., Lopes, C. S., Casares, F. and Iber, D.** (2016). A quantitative analysis of growth control in the Drosophila eye disc. *Development* **143**, 1482-1490.

**Wartlick, O., Jülicher, F. and Gonzalez-Gaitan, M.** (2014). Growth control by a moving morphogen gradient during Drosophila eye development. *Development* **141**, 1884-1893.

**Wolff, T. and Ready, D. F.** (1991). The beginning of pattern formation in the Drosophila compound eye: the morphogenetic furrow and the second mitotic wave. *Development* **113**, 841-850.

**Wright, V. M., Vogt, K. L., Smythe, E. and Zeidler, M. P.** (2011). Differential activities of the Drosophila JAK/STAT pathway ligands Upd, Upd2 and Upd3. *Cell. Signal.* **23**, 920-927.

**Zhang, Y., You, J., Ren, W. and Lin, X.** (2013). Drosophila glypicans Dally and Dally-like are essential regulators for JAK/STAT signaling and Unpaired distribution in eye development. *Dev. Biol.* **375**, 23-32.

## SUPPLEMENTARY MATERIALS AND METHODS

### Image reconstruction

*The description of the measurements in eye imaginal discs and of eye sizes in adult flies have been previously published in (Vollmer et al., 2016) and is repeated here for the convenience of the reader.*

To measure the eye discs in 3D, we first reconstructed the 3D apical surface of the developing eye disc. To this end, the apical membrane was manually segmented using the aPKC-antibody staining. Neighbouring membranes (the apposing peripodial epithelium), as well as parts belonging to the antenna were removed manually. Surface reconstruction and measurements of 3D areas were done using the commercial software package Amira. To measure the geometrical properties in 2D, maximum intensity projections were done as implemented in ImageJ (Abràmoff et al., 2004), and the areas as well as the posterior length (Fig. 1B,C, yellow line) were measured using the software ImageJ. The eye disc bends in 3D such that ventral "flaps" emerge below the 2D projection of the eye disc. We measured these separately and included these in the 2D measurements. 2D measurements were extrapolated to 3D given the linear correlation of those measures (Fig. S1).

Eye sizes of adult flies were measured using ImageJ. The heads of adult flies were mounted on Hoyer's:Lactic acid (1:1) mounting medium and cleared by overnight heating. Images were taken focusing on the front and back planes of the eye to account for all eye area. Front and back areas were summed up to give the total eye area.

The shape σ, given by the ratio of major to minor axis of an ellipse was determined, by fitting an ellipse to each eye disc such that the deviation between the measured anterior (A) and posterior (P) area and the ones predicted by an ellipse with the given posterior length $L_p$ and total area T was minimized.

**Computational analysis**

*The eye disc growth model has been described in detail before and the following description has been adapted from (Vollmer et al., 2016) for the convenience of the reader.*

Eye disc growth mainly occurs on the anterior side of the MF at rate $k(L_P)A$, where $k(L_P)$ is the area growth rate, $A$ the anterior area, and the posterior length $L_p$ serves as a measure of developmental time (Vollmer et al., 2016), as previous measurements established a linear relationship (Wartlick et al., 2014). Additionally, the area may change at rate $L_{MF}(L_P) \cdot (\phi - 1)$ as anterior area is converted into posterior area as a result of the MF movement. Here, $L_{MF}$ is the length of the morphogenetic furrow (MF) in dorsal-ventral direction. The total area increase can then be described by:

$$\frac{dT}{dL_P} = k(L_P)A + L_{MF}(L_P) \cdot (\phi - 1) \quad (5)$$

We previously showed that the second term has only a minor effect (Vollmer et al., 2016). Accordingly, we used $\Phi$=1 in all cases and thus assumed that differentiation does not alter the area. Please see (Vollmer et al., 2016) for a more detailed discussion on this. Moreover, we have

$$\frac{dP}{dL_P} = L_{MF}(L_P), \quad (6)$$

because the MF speed is $\frac{dL_P}{dL_P} = 1$ in our simulation framework. The measured MF speed, $v_{MF}$, can be used to convert the posterior length to real developmental time, as done for the simulations of the grafting experiments (Fig. 4C; $v_{MF}$= 3.4 µm/h as described in Vollmer et al., 2016). The anterior area follows as

$A = T - P$.

Since the shape of the eye disc can be approximated by an ellipse (Vollmer et al., 2016), we can use the equations for an ellipse,

$$A = T\left[1 - \frac{1}{\pi}\left(\cos^{-1}\left(1 - \frac{2L_P}{L_{AP}}\right) - 2\left(1 - \frac{2L_P}{L_{AP}}\right)\sqrt{\frac{L_P}{L_{AP}}\left(1 - \frac{L_P}{L_{AP}}\right)}\right)\right] \quad (7)$$

to calculate the current shape of the eye disc given the current values for T, A, and $L_p$. Here $L_{AP}$ is the total length of the disc in anterior-posterior direction. The minor axis of length $a$ then follows as $a = L_{AP}/2$, and the major axis of length $b$ as $b = T/\pi a$. $L_{MF}(L_P)$ can then be determined accordingly.

Eqs. (5-7) can be simulated with any growth law $k(L_P)$, including for growth control based on pure dilution as given by Eq. 2

$$k(L_P) = k_0 \frac{T(0)}{T(L_P)},$$

or a dilution model with added degradation as given by Eq. 4

$$k(L_P) = k_0 \frac{T(0)}{T(L_P)} e^{-\delta(L_P - L_P(0))}.$$

We start the simulations with an initial posterior length $L_{p0}$=15μm. All other parameters for the models were optimized such that the deviation of the model from the measured area distributions for T, P and A (Fig. 1C,D) was minimized. A trust-region-reflective algorithm (Coleman and Li, 1996) was used as implemented in the lsqnonlin function in the commercial software Matlab R2016a. For ODE integration we used a forward Euler scheme.

**Simulation of Transplant Experiments**

Eye disc growth is substantially slower when eye discs are transplanted to the abdomen of adult flies, but similar final disc sizes are obtained (Garcia-Bellido, 1965). Given the longer developmental times, we checked whether a dilution model could still reproduce the observed growth kinetics with the needed Upd half-life of 24 hours (Fig. 2). In the reported experiments, 24 hours AEL, the 4 most anterior segments of larvae were transplanted without the brain to the abdomen of 4-day old virgin (squares, dashed line) or fertilized flies (circle, dashed line), or with brain to fertilized flies (triangles, solid line) (Garcia-Bellido, 1965). In the more slowly growing eye discs, the MF must move at a slower speed; we need to reduce $v_{MF}$ to 5% of the value used in *GMR*>+. The maximal growth rate, $k_0$, needs to be reduced only to 28% of the value used for *GMR*>+. If the half-life is assumed to be 48 hours, $v_{MF}$ needs to be reduced to 5% and $k_0$ to 18%. Relative values are given with respect to Table S1.

**Fluorescence recovery after photobleaching**

*The experimental procedure for FRAP measurements has been described before and the following part has been adapted from (Fried et al., 2016) for the convenience of the reader.*

Imaginal discs were dissected in SF-900 medium at room temperature (21°C), and transferred to a medium-containing well with a glass coverslip bottom. The samples were maintained at 21°C. The data analysis was done using different software applications. For the imaging analysis ImageJ v.1.47f was used; the statistics was done using the Microcal Origin v.8.1 software.

To determine the Upd diffusion coefficient, eye imaginal discs from GMR-GAL4; UAS-GFP:Upd were used (Tsai and Sun, 2004). The ROI (solid circle with a radius of 5.7 µm in Fig. 3A) was photobleached for 46 s using an Argon laser 488 nm with laser power 36.8% and transmission 100%. The recovery was observed by exciting GFP in the sample with an Argon laser 488 nm with laser power 2% and transmission 100%, pinhole 1.4 Airy units. The laser was installed on a confocal microscope Nikon Ti with 60x(1.40) VC OIL DIC objective using a camera Nikon A1, zoom 2.5x, gain ~1200. The movies have a duration of 10 min with one frame every 4 seconds, each frame with a 2-line average.

The number of samples taken to perform this analysis was n = 9. The image analysis was performed following the description in (Kang et al., 2012). Here the diffusion coefficient is defined as:

$$D = \frac{r_e^2 + r_n^2}{8 \cdot \tau_{1/2}}$$

where $r_n$ is the nominal radius (ROI radius), $r_e$ is the effective radius (spreading radius of postbleached profile) and $\tau_{1/2}$ is the half time of the recovery. In order to calculate $r_e$, the bleaching profile (Fig. 3F) can be approximate by an Gaussian profile fitting it to the following expression:

$$f(x) = 1 - K \cdot \exp\left(\frac{-x^2}{r_e^2}\right)$$

$K$ and $r_e$ can be obtain using a nonlinear least-squares fitting routing (nlinfit.m) available in MATLAB.

These parameters can also be obtained by applying a direct protocol. First, $K$ can be determined from the bleaching depth in the normalized postbleach profile as referred to in Fig. 3B. Then, the half width of cross-sections between the horizontal line at the height of $0.86K$ from the bottom of the postbleach profile (Fig. 3B) and the postbleach profiles yields $r_e$ without involving any fitting (Fig. 3B).

To measure $\tau_{1/2}$ from the FRAP data a linear interpolation method was used. $F:\{F(0),F(t_1),F(t_2),\cdots,F(t_n)\}$ such that $F(0)=F0$ and $F(t_n)=F^{\infty}$. The fluorescence intensity at half of recovery is defined as $F_{1/2}=\left(F0+F^{\infty}\right)/2$. If $F(t_k)=F_{1/2}$ for some $t_k$ then the half-recovery time follows as $\tau_{1/2}=t_k$. If $F(t_k)<F_{1/2}<F(t_{k+1})$ it is defined as:

$$\tau_{1/2} = t_k + \frac{F_{1/2}-F(t_k)}{F(t_{k+1})-F(t_k)}(t_{k+1}-t_k)$$

Figure 3A shows one of the eye discs where the photobleaching was done. Figures 3B-E show some photobleaching recovery frames with details. A bleaching profile sample can be observed in figure 3F and the bleaching recovery profile is shown in figure 3G. According to the analysis the half recovery time is of $\tau_{1/2}$ = 1.3 min and the diffusion coefficient was calculated as $D_{Upd}$= 0.67 ± 0.19 μm$^2$ s$^{-1}$.

*Notes on protocol:*

We used an ectopically expressed GFP-tagged form of Upd to determine the diffusion coefficient and diffusion length of Upd, which allows us to infer the half-life of the Upd protein. We used Fluorescence Recovery After Photobleaching (FRAP) rather than Fluorescence Correlation Spectroscopy (FCS) to determine the diffusion coefficient, because in this way we obtain the effective diffusion coefficient over a wider distance rather than the local diffusion coefficient. Measurements by FRAP require the expression of a fluorescently-tagged protein, and all previous FRAP-based measurements of diffusion coefficient of morphogens in Drosophila imaginal discs have been carried out by overexpressing the fluorescently-tagged protein of interest (Kicheva et al., 2007). We acknowledge that saturation effects due to ligand overexpression may increase the diffusion coefficient compared to the wildtype situation such that the wildtype diffusion coefficient would be smaller. However, in case of a larger diffusion coefficient, also the diffusion length would be increased (which we establish with the same construct). As we are only interested in the degradation rate/half-life, the two effects will cancel.

Overexpression of a protein can, in principle, lead to either the generation of an abnormal form with altered half-life, or to the accumulation of a receptor-unbound form that could be more stable. However, overexpression of Upd has been shown to be active, and its molecular structure is therefore presumably preserved (Bach et al., 2003). Second, the genetic system that we use (GAL4/UAS) does not lead to saturating levels of Upd. Thus, GAL4/UAS is temperature sensitive, and the experiments for the determination of the molecular properties of Upd were carried out at 25ºC. In the range of temperatures that we use (18-29 ºC), increasing temperature (i.e. Upd production) also increases the severity of the phenotype, indicating that at 25ºC the receptor and its signaling pathway is not saturated (Fig. S8). Finally, we have now extended our previously published computational model of eye disc patterning (Fried et al., 2016) to study the effect of constitutive Upd production behind the

MF (Gmr>Upd) (Fig. S5). If we assume that the ectopic production rate of Upd per unit area is the same as the endogenous one in the posterior rim before the MF starts, then the model predicts that in the Gmr>Upd genotype, the maximal Upd concentration never exceeds the maximal Upd concentration in the control strain – so that receptor saturation will not be a problem. The reason for this observation is that a substantial ectopic production of Upd only starts with a delay when the MF has sufficiently advanced to create a sizeable posterior area. By that time, the endogenous Upd concentration has, however, already strongly declined as a result of dilution. In conclusion, saturation should not be a problem, and we expect the GFP-tagged ectopically expressed Upd to have a similar half-life as the endogenous Upd.

## Supplementary Tables

**Supplementary Table S1:** Parameter values for *Gmr>+*, all models with $L_P(0)$ = 15 µm.

| Model | $k(L_P)$ | T(0) [µm$^2$] | $k_0$ [µm$^{-1}$] | σ(0) | δ [µm$^{-1}$] |
|---|---|---|---|---|---|
| **P_A** | $k(L_P) = k_0 \frac{T(0)}{T(L_P)}$ | 1.4794E+04 | 0.0812 | 5.7206 | - |
| **P_A, 6h** | $k(L_P) = k_0 \frac{T(0)}{T(L_P)} e^{-\delta(L_P - L_P(0))}$ | 1.0844e+04 | 0.1903 | 5.6566 | 0.0158 |
| **P_A, 12h** | $k(L_P) = k_0 \frac{T(0)}{T(L_P)} e^{-\delta(L_P - L_P(0))}$ | 1.2233e+04 | 0.1335 | 5.8116 | 0.0079 |
| **P_A, 24h** | $k(L_P) = k_0 \frac{T(0)}{T(L_P)} e^{-\delta(L_P - L_P(0))}$ | 1.3321e+04 | 0.1064 | 5.8121 | 0.0040 |
| **P_A, 36h** | $k(L_P) = k_0 \frac{T(0)}{T(L_P)} e^{-\delta(L_P - L_P(0))}$ | 1.3764e+04 | 0.0978 | 5.7934 | 0.0026 |
| **P_A, 48h** | $k(L_P) = k_0 \frac{T(0)}{T(L_P)} e^{-\delta(L_P - L_P(0))}$ | 1.4003e+04 | 0.0935 | 5.7798 | 0.0020 |
| **P_A, 72h** | $k(L_P) = k_0 \frac{T(0)}{T(L_P)} e^{-\delta(L_P - L_P(0))}$ | 1.4254e+04 | 0.0894 | 5.7633 | 0.0013 |
| **P_A, 96h** | $k(L_P) = k_0 \frac{T(0)}{T(L_P)} e^{-\delta(L_P - L_P(0))}$ | 1.4384e+04 | 0.0873 | 5.7538 | 9.89e-04 |
| **EXP** | $k_0 e^{-\delta(L_P - L_P(0))}$ | 1.5595E+04 | 0.0555 | 5.5309 | 0.0168 |

## Supplementary Figures

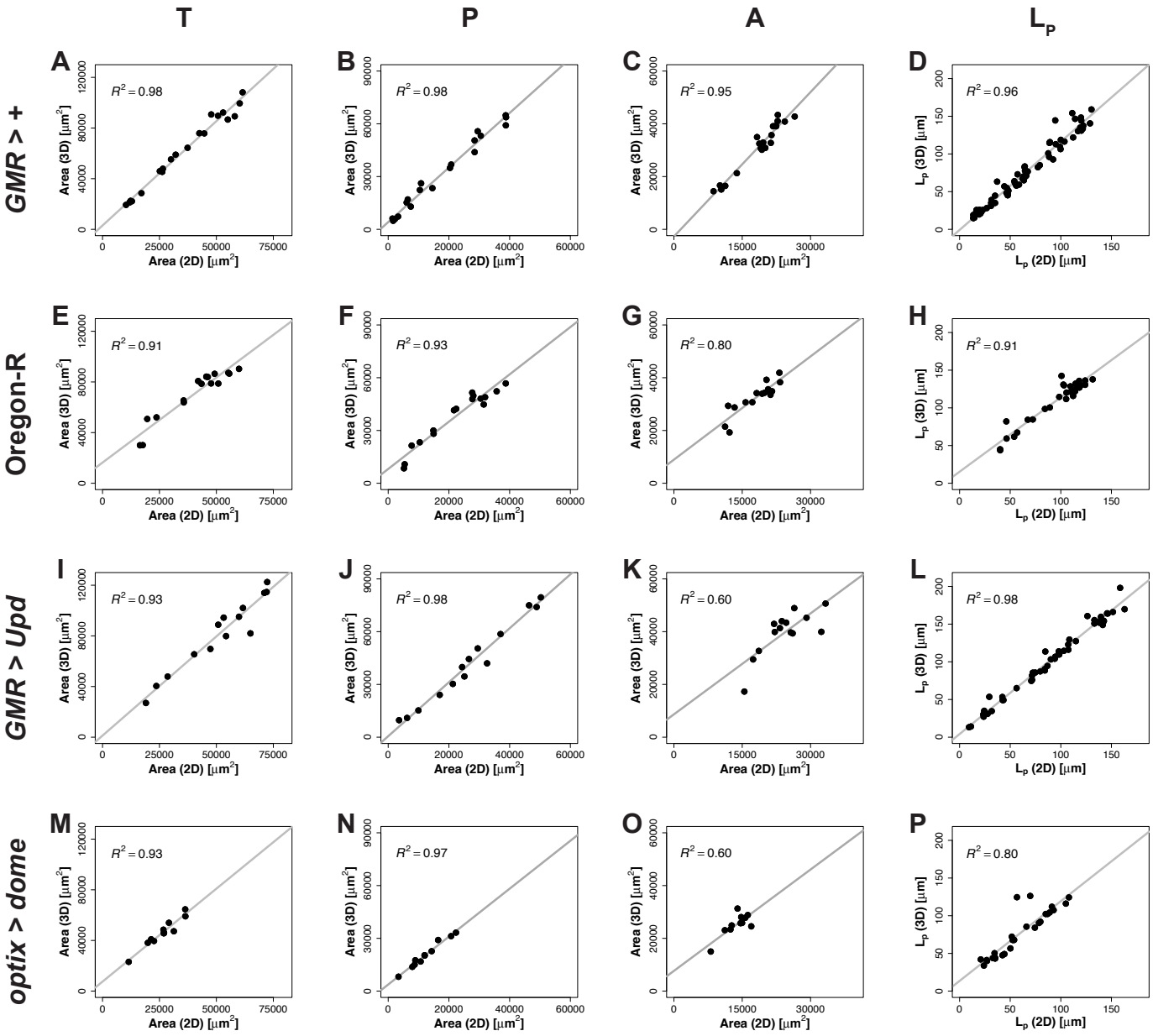


**Figure S1: Correlations of 2D and 3D measurements**

Linear correlation for the 2D and 3D measurements of total area (first column, A,E,I,M), posterior area (second column, B,F,J,N), anterior area (third column, C,G,K,O) and posterior length $L_P$ (last column, D,H,L,P).

(A-D) Data for *GMR>+*. This data was taken from (Vollmer et al., 2016).

(E-H) Data for Oregon-R. This data was taken from (Vollmer et al., 2016).

(I-L) Data for *GMR>Upd*

(M-P) Data for *optix>dome*

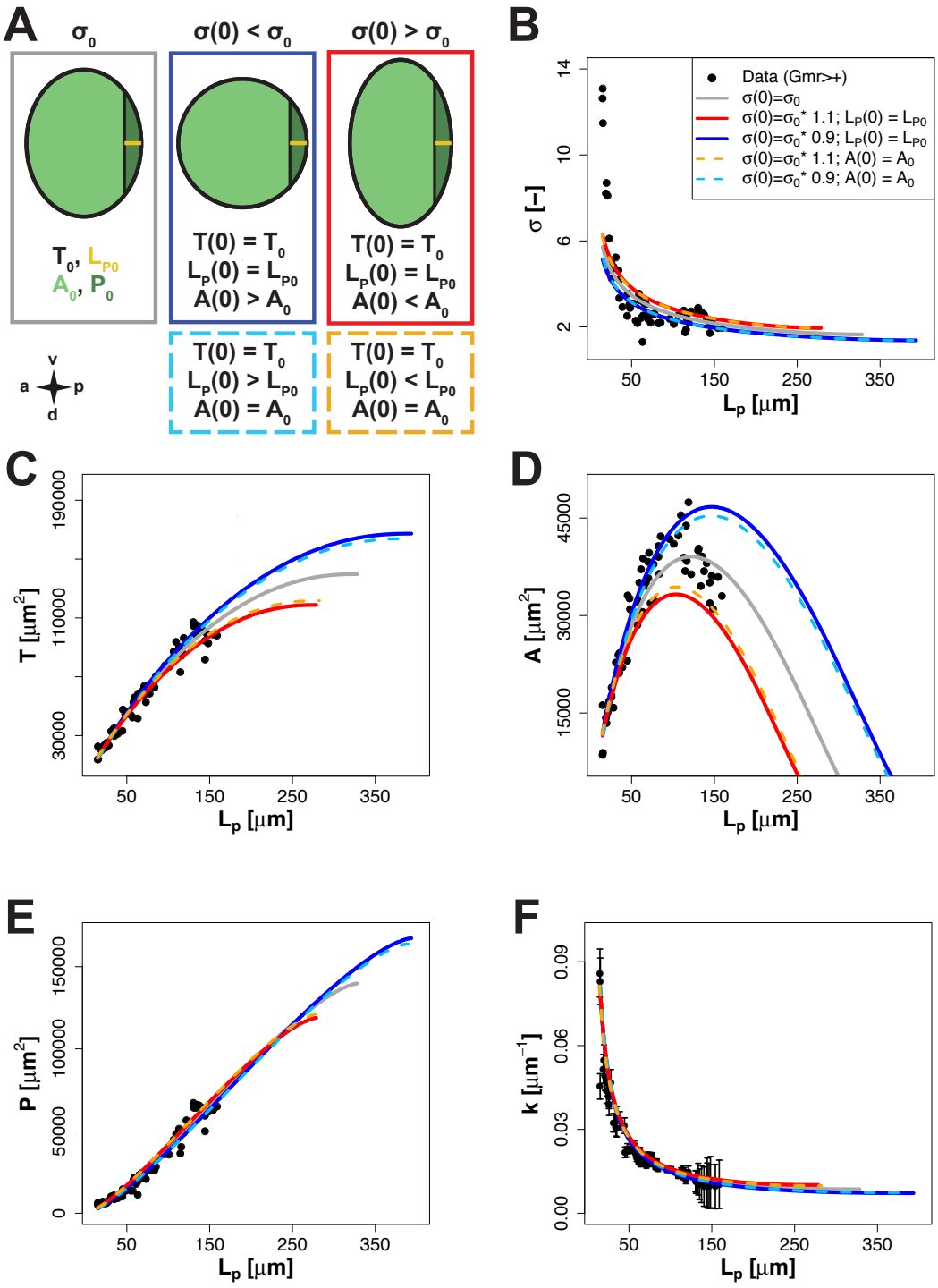

**Figure S2: Impact of the initial shape on the growth kinetics and final size**

To show the impact of the initial shape on the growth kinetics and the resulting final size, the initial shape was changed by 10% to a more elongated ($1.1 * \sigma_0$) or rounder ($0.9 * \sigma_0$) shape while keeping the initial total area $T_0$ constant. Here $\sigma_0$, $L_{P0}$, $T_0$, $A_0$ and $P_0$ refer to the initial shape, the initial posterior length and the initial total, anterior and posterior area obtained from fitting the *GMR>+* data set.

The area growth rate was assumed to follow the area-dependent decline (Eq. 2). The parameter values for the *GMR>+* data set were taken as the reference (supplementary table 1).

In a first case, the initial posterior length $L_P(0)$ and the initial total area $T_0$ were kept constant. As a consequence, the values for the initial anterior area A(0) and the posterior area P(0) were different (coloured solid lines) from the reference simulation ($A_0$, $P_0$, grey line). In a second case, the initial total area $T_0$ as well as the initial anterior (A(0)) and posterior (P(0)) areas were kept constant by modifying the initial posterior length $L_P(0)$ (coloured dashed lines), i.e. $A(0)= A_0$, $P(0)= P_0$ and $L_P(0)<L_{P0}$.

(A) Visualization of the different initial conditions chosen for the simulations.

(B-F) Growth kinetics for the different initial shapes and area distributions. Black dots: data for *GMR>+*; Grey line: reference simulation with parameters $\sigma_0$, $T_0$, $A_0$ obtained from fitting the *GMR>+* data set; Solid coloured lines: Varied shape, $L_p(0)$ as in the reference simulation; Dashed lines: Varied shape, area distribution as in the reference simulation.

A rounder initial shape (B-F, blue lines) leads to a bigger final total area independent of which measure ($L_p(0)$ or initial area distribution) is conserved.

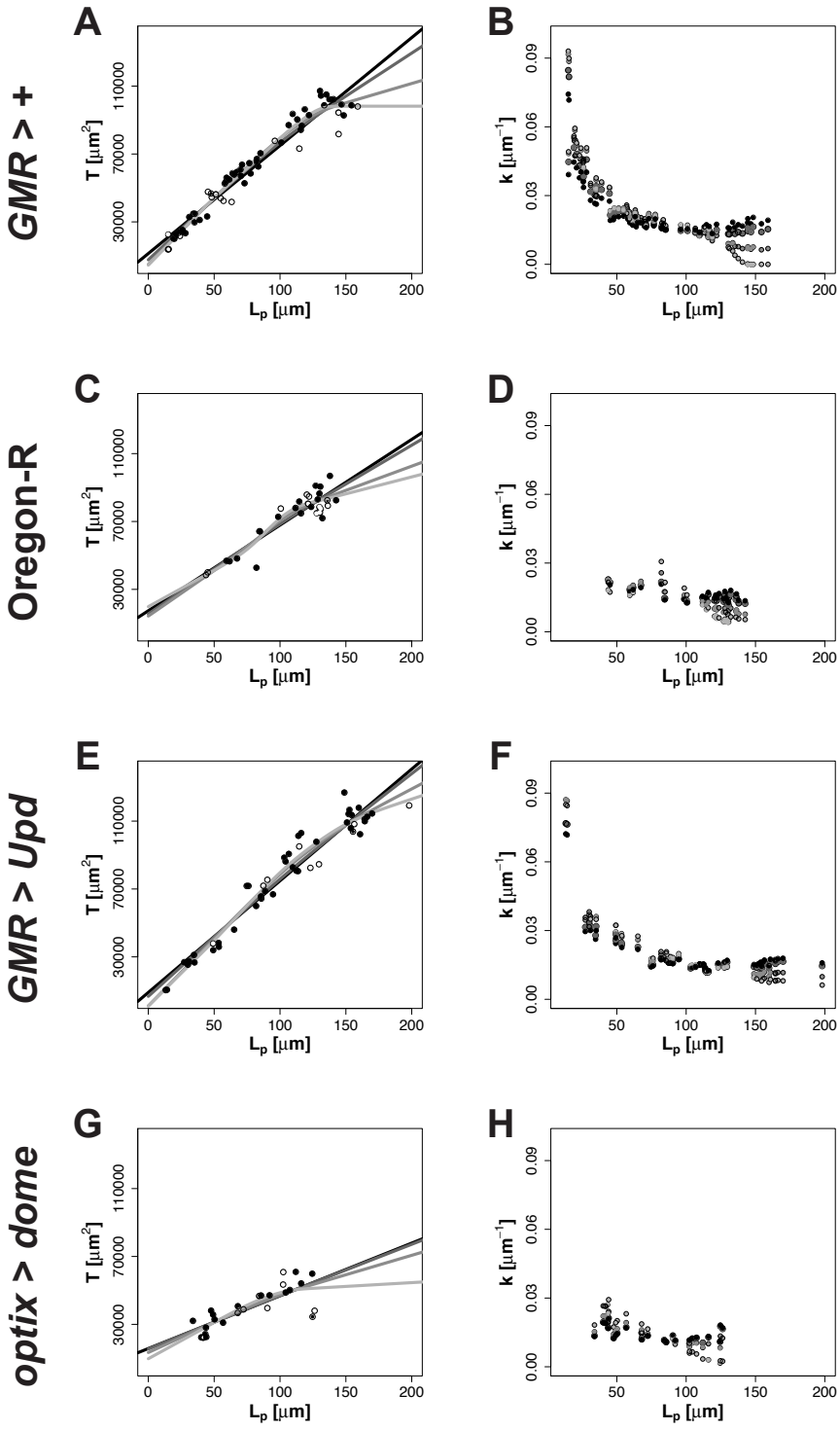


**Figure S3: Estimation of area growth rates from the data**

To estimate the area growth rates k from the data for the different genotypes, we used the same approach as described in (Vollmer et al., 2016) and Supplementary Text S2. The area growth rate *k* follows from

$$\frac{dT}{dL_P} = k(L_P) * A.$$

The area growth rate *k* can thus be obtained by dividing the slope in the total area T versus posterior length $L_P$ plot by the respective anterior area A.

The genotypes are: (A,B) *GMR>+*; (C,D) Oregon-R; (E,F) *GMR>Upd*; (G,H) *optix>dome*;

(A,C,E,G) For each genotype, a linear model (black lines) as well as spline fits (grey lines) with varying degrees of freedoms were used to fit the increase of the total area T. Spline fits were used since the data might not be fitted perfectly using a linear model. The uncertainty in the estimate of the area growth rate *k* is thus highest where the models deviate most (see second column).

(B,D,F,H) The slope of the fits from the linear model and spline fits was divided by the anterior area A to obtain the area growth rate k. The colour code refers to the fits from the first column.

Data presented in panels (A)-(D) was taken from (Vollmer et al., 2016).

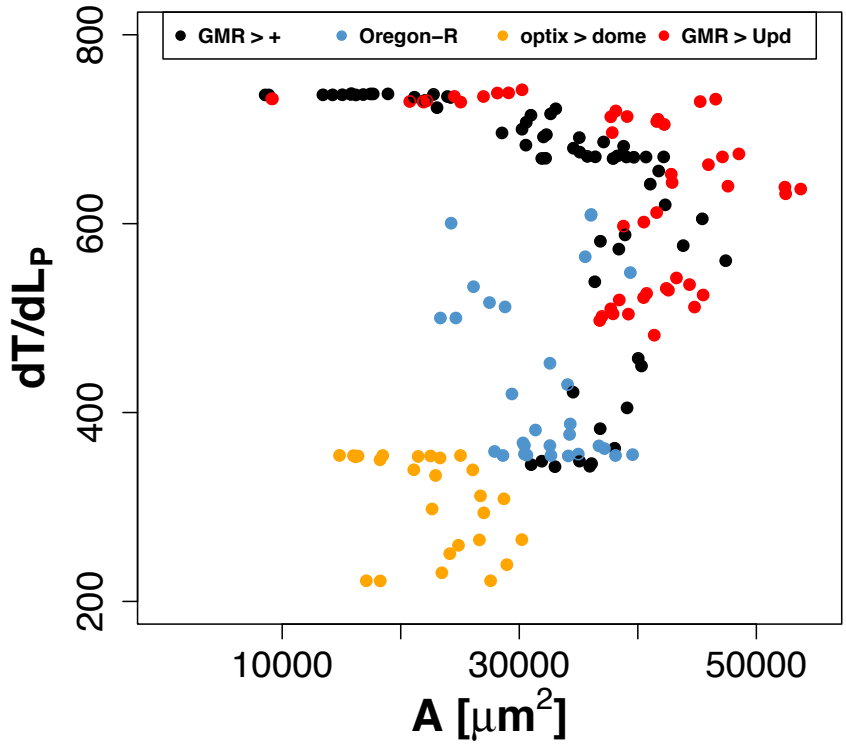


**Figure S4: Growth kinetics in the different genotypes**

Inferred average slope of the increase of the total area T with the posterior length $L_p$ (Fig. S3) plotted versus the respective anterior area $A$ for *GMR>+* (black), Oregon-R (blue), *optix>dome* (yellow) and *GMR>Upd* (red). The different genotypes fall into distinct regions in the plots, with some overlay of *GMR >+* and *GMR >UPD*.

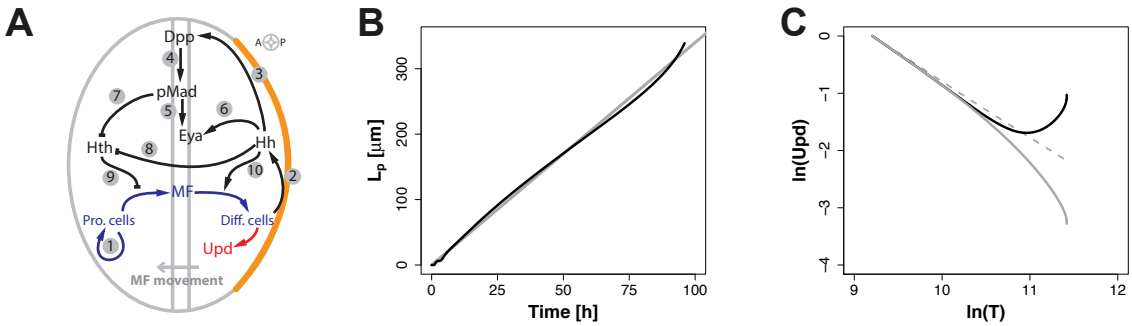


**Figure S5: Impact of Upd production posterior to the MF on the Upd concentration in the eye disc**

To model the impact of Upd production posterior to the MF, as is the case in the *GMR>Upd* genotype, we adapted a version of our model for eye disc patterning (Fried et al., 2016). All model parameters were kept as in the published version, but an Upd species was included that is produced by the differentiated cells Φ posterior to the MF (the domain of GMR-GAL4 expression). The initial concentration of Upd was set to 1 [a.u.]. Its concentration was assumed to be in steady state at the beginning of the simulation, i.e. when the MF starts to move. The growth rate was set to be directly proportional to the concentration of Upd. The initial (maximal) growth rate $k_0$ was set to the previously inferred value 0.0812 1/µm (Vollmer et al., 2016). As before (Fried et al., 2016), we modelled the growth of the eye disc using an incompressible Newtonian fluid. The Navier-Stokes equation is given as

$$\rho\left(\frac{\partial u}{\partial t} + (\nabla \cdot u)u\right) = -\nabla \mathrm{p} + \mu(\nabla^2 u + \frac{1}{3}\nabla(\nabla \cdot u))$$

$$\nabla \cdot u = S = \Pi \cdot k_0 \cdot c_{Upd}$$

with fluid density ρ, dynamic viscosity µ, and the local source or growth rate *S*. *u* denotes the fluid velocity field and $c_{Upd}$ the concentration of *Upd*. Π denotes the area occupied by the proliferating cells, i.e. the area anterior to the MF. Additionally, Upd was set to be degraded everywhere in the disc with a half-life of 24 hours as inferred in this manuscript (Fig. 4), such that $\delta_{Upd} = \ln(2)/24$ [1/h]. Since the model was originally adapted to fit the speed measured by (Wartlick et al., 2014), the decay constant was adapted to the speed determined for Gmr>+ (Fig. 2A,B). The production rate was taken to be same as for the endogenous Upd that is produced before the start of the MF movement. As we use a Upd initial concentration of 1,

the endogenous production rate follows as $p_{Upd} = \delta_{Upd}$. The Upd diffusion coefficient was set to $D_{Upd}$=0.7 μm$^2$/s, as determined by FRAP in this manuscript (Fig. 3). In summary, we model the spatio-temporal evolution of all model components $c_i$ using reaction-advection-dispersion equations according to

$$\frac{\partial c_i}{\partial t} + \nabla(\mathrm{u}c_i) = D_i \nabla^2 c_i + R_i.$$

The reaction term $R_i$ for the Upd species in the GMR>Upd genotype reads

$$R_{Upd}^{Gmr>Upd} = \phi \cdot p_{Upd} - \delta \cdot c_{Upd}$$

, and for the Gmr>+ genotype,

$$R_{Upd}^{Gmr>+} = -\delta \cdot c_{Upd}.$$

(A) Complete model as published by (Fried et al., 2016) with the additional species Upd (marked in red).

(B) The MF moves about linearly with time in the model for the GMR>Upd genotype (black) and closely matches the position of an MF that advances at the previously measured speed of 3.4 μm/h (Vollmer et al., 2016; Wartlick et al., 2014).

(C) ln-ln plot of the Upd concentration at the center of the disc versus the total area $T$ for three different genotypes. Black, solid line: A model of the GMR>Upd genotype. Upd is degraded, diluted and produced behind the MF. Grey, dashed line: Pure Dilution. A theoretical species that gets only diluted, but neither produced nor degraded. Grey, solid line: A model of the GMR>+ genotype. Upd gets diluted and degraded, but not produced. In all three cases, the concentration drops initially, mainly due to the growth and thus due to dilution, before production of Upd posterior to the MF can start and counteract the dilution and degradation. The biggest differences can only be observed towards the end of eye development. At this stage, pupation starts and no data could be obtained.

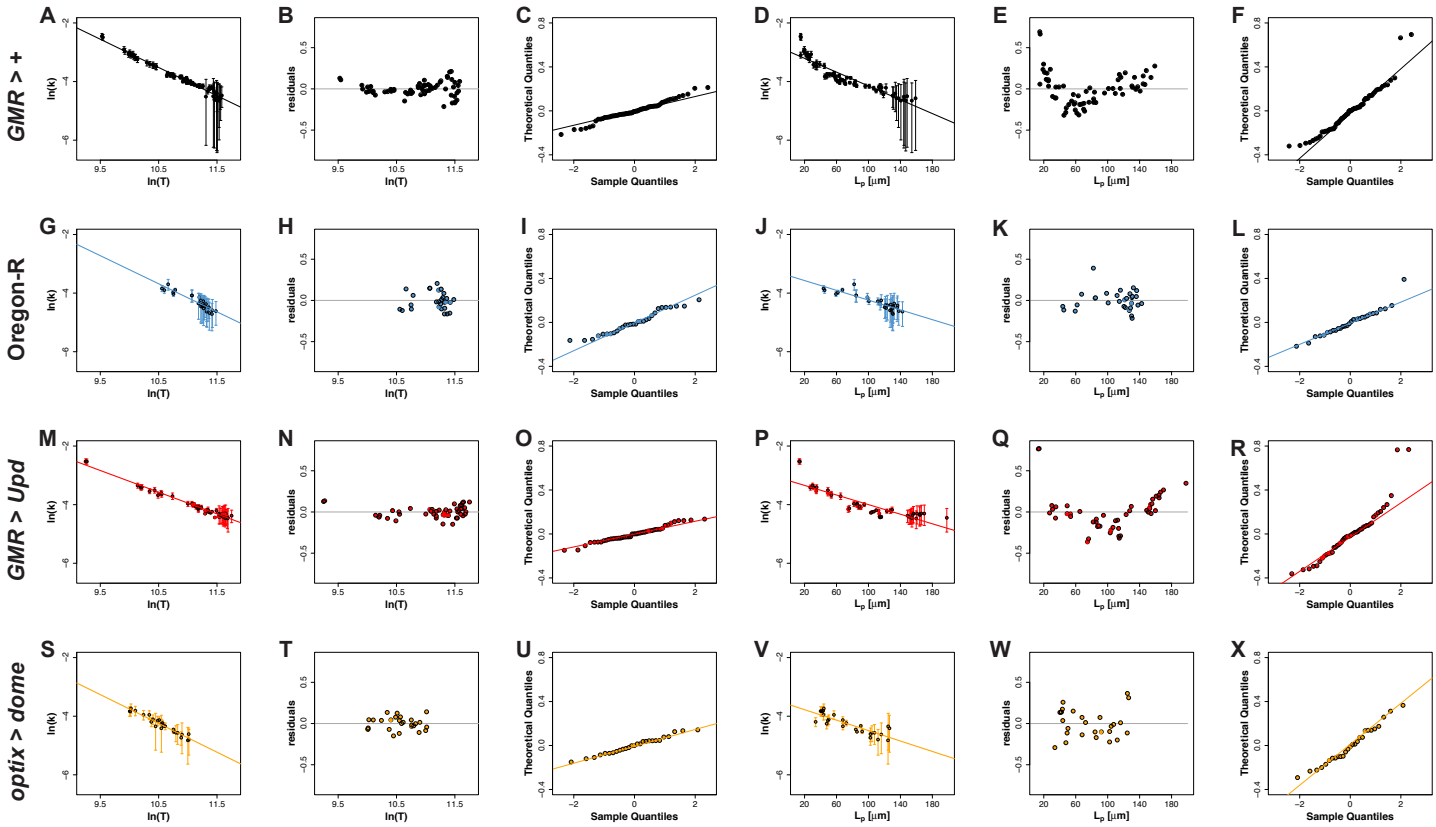


**Figure S6: Residuals and analysis of the normality of the linear fits to the area growth rate *k***

Fit, residuals and QQ-plot for ln(k) versus ln(T) and ln(k) versus $L_P$ for the data sets of the different genotypes.

(A-F) *GMR>+*; (G-L) Oregon-R; (M-R) *GMR>Upd*; (S-X) *optix>dome*

A systematic trend with the highest positive deviations of the residuals at small and big posterior lengths $L_P$ and negative deviations at intermediate posterior lengths can be seen for the *GMR>+* and *GMR>Upd* data set when fitting a linear model to ln(k) versus $L_P$ (panels E and K).

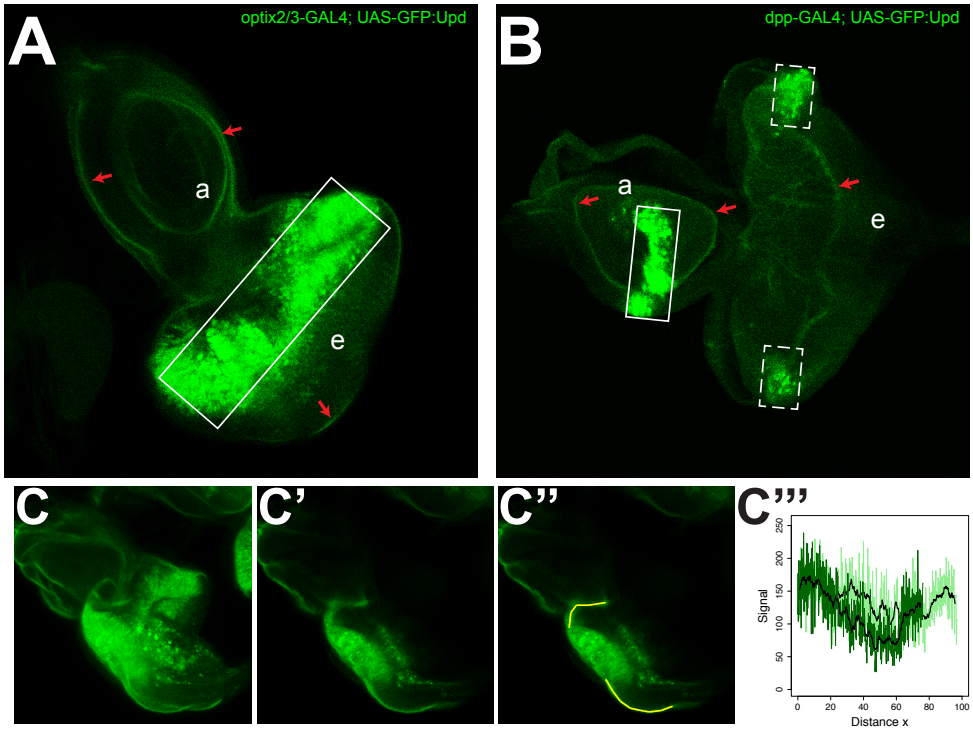


**Figure S7: Expression of GFP:Upd in different domains of the eye–antennal disc results in uniform and widespread dispersion of GFP:Upd.**

Eye-antennal imaginal discs expressing GFP:Upd under the control of different GAL4 drivers (A,B). The expression domains are marked by white boxes. (A) *optix2/3-GAL4; UAS-GFP:Upd*. GFP:Upd is expressed in a central region of the eye disc; (B) *dpp$^{blk}$-GAL4; UAS-GFP:Upd*. GFP:Upd is produced in an antennal domain (boxed, solid line) and in two weaker lateral eye domains (boxed, dashed line). In both genotypes, and in addition to the production domains, GFP:Upd is detected with uniform intensity on the apical surface of the epithelium. Red arrows point to some of these epithelial surfaces. "a" antennal disc region; "e" eye disc region. Anterior is left and dorsal is up in (A,B). The *optix2/3-GAL4* and *dpp$^{blk}$-GAL4* driver lines are described in (Neto et al., 2016; Ostrin et al., 2006) and (Staehling-Hampton et al., 1994), respectively. (C-C''') Lateral view of an eye imaginal disc where GFP:Upd is expressed under the control of optix2/3. (C) Maximum intensity projection; (C') Single image plane; (C'' and C'''') Quantification of the intensity profile along the marked lines (yellow, C'') into posterior direction (light green) and anterior direction (dark green). Raw profiles (coloured) and moving average (black) are shown. The intensity profiles overlap arguing against a directed movement of GFP:Upd.

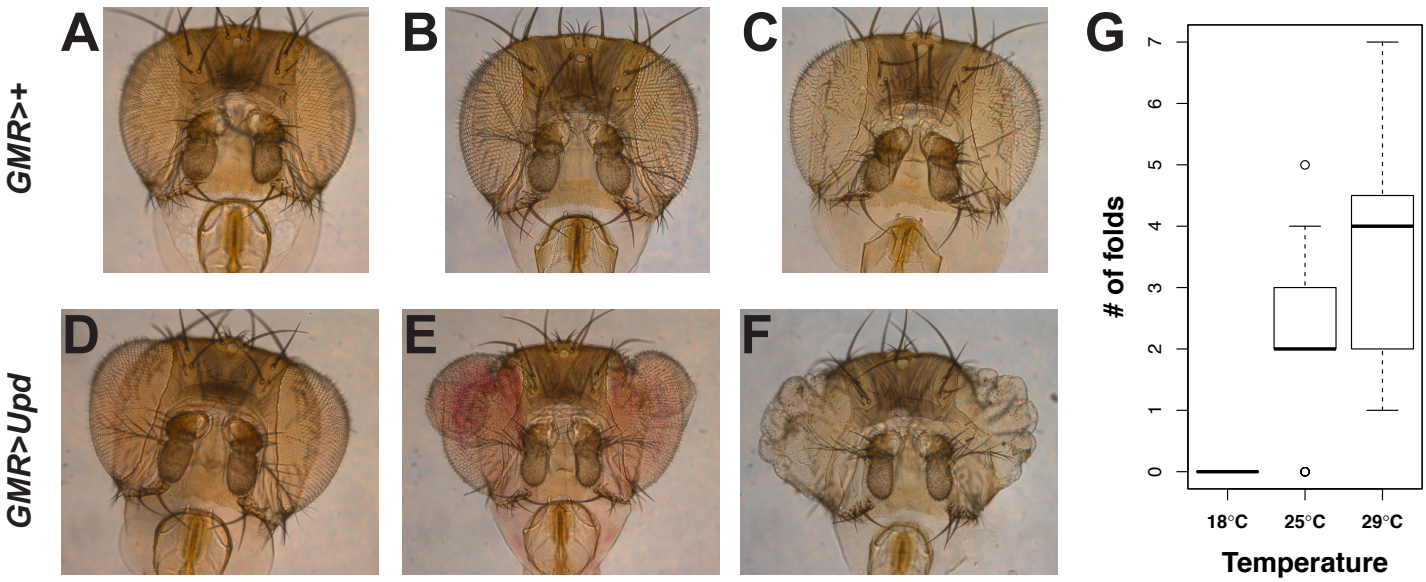


**Figure S8: The eye overgrowth phenotype is temperature sensitive between 18°C and 29°C**

Control (*Gmr>+*) and flies with *upd* expression driven by the *GMR*-GAL4 line in differentiated cells (*GMR>Upd*) were raised at 18°C (A, D), 25°C (B,E), and 29°C (C,F). While there are no big changes of eye sizes in adult flies for the control strain (A-C), there is a clear increase in the eye overgrowth with higher temperatures in the *GMR>Upd* genotype (D-F). This indicates that signalling downstream of Upd is not saturated at the intermediate temperature of 25°C, at which the experiments for the determination of the molecular properties of Upd were carried out. Due to the massive overgrowth, folding of the adult eye occurs in the *GMR>Upd* genotype (D-F). Thus, eye area as previously measured in 2 dimensions on flat images (Fig. 1A), is not an appropriate measure anymore, as it cannot account for the increased area due to the folding. Therefore, numbers of folds were used as a measure of overgrowth for the *GMR>Upd* genotype instead (H). Visual inspection (D-F) and numbers of folds (H) confirm the sensitivity of the system at increasing temperatures. Number of flies analysed for panel H: 18°C, n=11; 25°C, n=12; 29°C, n=9; Panels A-F are representative sample images from the flies analysed.

## REFERENCES

**Abràmoff, M. D., Magalhães, P. J. and Ram, S. J.** (2004). Image processing with ImageJ. *Biophotonics Int.* **11**, 36–42.

**Bach, E. a, Vincent, S., Zeidler, M. P. and Perrimon, N.** (2003). A sensitized genetic screen to identify novel regulators and components of the Drosophila janus kinase/signal transducer and activator of transcription pathway. *Genetics* **165**, 1149–66.

**Coleman, T. F. and Li, Y.** (1996). An Interior Trust Region Approach for Nonlinear Minimization Subject to Bounds. *SIAM J. Optim.* **6**, 418–445.

**Fried, P., Sánchez-Aragón, M., Aguilar-Hidalgo, D., Lehtinen, B., Casares, F. and Iber, D.** (2016). A Model of the Spatio-temporal Dynamics of Drosophila Eye Disc Development. *PLoS Comput. Biol.* **12**, e1005052.

**Garcia-Bellido, A.** (1965). Larvalentwicklung transplantierter Organe von Drosophila melanogaster im Adultmilieu. *J. Insect Physiol.* **11**, 1071–1078.

**Kang, M., Day, C. A., Kenworthy, A. K. and DiBenedetto, E.** (2012). Simplified equation to extract diffusion coefficients from confocal FRAP data. *Traffic* **13**, 1589–600.

**Kicheva, A., Pantazis, P., Bollenbach, T., Kalaidzidis, Y., Bittig, T., Jülicher, F. and González-Gaitán, M.** (2007). Kinetics of morphogen gradient formation. *Science* **315**, 521–5.

**Neto, M., Aguilar-Hidalgo, D. and Casares, F.** (2016). Increased avidity for Dpp/BMP2 maintains the proliferation of progenitors-like cells in the Drosophila eye. *Dev. Biol.* **418**, 98–107.

**Ostrin, E. J., Li, Y., Hoffman, K., Liu, J., Wang, K., Zhang, L., Mardon, G. and Chen, R.** (2006). Genome-wide identification of direct targets of the Drosophila retinal determination protein Eyeless. *Genome Res.* **16**, 466–476.

**Staehling-Hampton, K., Jackson, P. D., Clark, M. J., Brand, A. H. and Hoffmann, F. M.** (1994). Specificity of bone morphogenetic protein-related factors: Cell fate and gene expression changes in Drosophila embryos induced by decapentaplegic but not 60A. *Cell Growth Differ.* **5**, 585–593.

**Tsai, Y.-C. and Sun, Y. H.** (2004). Long-range effect of upd, a ligand for Jak/STAT pathway, on cell cycle in Drosophila eye development. *Genesis* **39**, 141–53.

**Vollmer, J., Fried, P., Sánchez-Aragón, M., Lopes, C. S., Casares, F. and Iber, D.** (2016). A quantitative analysis of growth control in the Drosophila eye disc. *Development* **143**, 1482–90.

**Wartlick, O., Jülicher, F. and Gonzalez-Gaitan, M.** (2014). Growth control by a moving morphogen gradient during Drosophila eye development. *Development* **141**, 1884–93.